Atmos. Chem. Phys. Discuss., 14, 13233–13269, 2014
www.atmos-chem-phys-discuss.net/14/13233/2014/
doi:10.5194/acpd-14-13233-2014
© Author(s) 2014. CC Attribution 3.0 License.

Atmospheric Chemistry and Physics Discussions

This discussion paper is/has been under review for the journal Atmospheric Chemistry and Physics (ACP). Please refer to the corresponding final paper in ACP if available.

On the relationship between responses in cloud water and precipitation to changes in aerosol

Z. J. Lebo[1,2] **and G. Feingold**[2]

[1]Cooperative Institute for Research in Environmental Sciences, University of Colorado Boulder, Boulder, Colorado, USA
[2]Chemical Sciences Division, NOAA Earth System Research Laboratory, Boulder, Colorado, USA

Received: 29 April 2014 – Accepted: 9 May 2014 – Published: 22 May 2014

Correspondence to: Z. J. Lebo (zach.lebo@noaa.gov)

Published by Copernicus Publications on behalf of the European Geosciences Union.

Abstract

Climate models continue to exhibit strong sensitivity to the representation of aerosol effects on cloud reflectance and cloud amount. This paper evaluates proposed efforts to constrain modeled cloud liquid water path (LWP) adjustments in response to changes in aerosol concentration N_a using observations of precipitation susceptibility. Recent climate modeling has suggested a linear relationship between relative LWP responses to relative changes in N_a (i.e., $\mathrm{d}\ln\mathrm{LWP}/\mathrm{d}\ln N_a$) and the precipitation frequency susceptibility S_{pop}, defined as the relative change in the probability of precipitation for a relative change in N_a. A satellite-based measurement of S_{pop} combined with this model–based relationship provide a constraint on $\mathrm{d}\ln\mathrm{LWP}/\mathrm{d}\ln N_a$. Through a review of the existing literature and a suite of large eddy simulations of stratocumulus and trade-wind cumulus clouds, we show that the climate model–based relationship is not unique and sometimes even has an opposite slope to those from fine-scale studies. Therefore, we propose a more careful examination of the scale and regime dependence of this relationship.

1 Introduction

Like its predecessors, the IPCC Fifth Assessment Report (AR5; IPCC 2013) continues to point to aerosol effects on clouds as a major source of uncertainty in our predictive climate modeling capability. Recognizing that cloud systems constantly adjust to aerosol perturbations, AR5 chose to combine both cloud albedo and LWP responses to aerosol changes into one term, i.e., the effective radiative forcing associated with aerosol-cloud interactions (ERFaci). The representation of the underlying microphysical processes associated with cloud formation and albedo and precipitation modification must be improved to better quantify ERFaci. Attempts to constrain ERFaci with observations is an important part of this quantification. Early efforts (e.g., Quaas et al., 2006, 2009) used satellite-based measurements of drop concentration

ACPD
14, 13233–13269, 2014

(or size) responses to changes in aerosol (Bréon et al., 2002) to constrain the albedo effect (Twomey, 1977). More detailed analysis using surface-based remote sensing and proxy data from cloud resolving models pointed to the scale dependence of these relationships (McComiskey and Feingold, 2008, 2012) and called for a clear distinction between the cloud process scale and the satellite data aggregation scale before such observational constraints are applied.

In this paper, we shift attention to observational constraints on aerosol effects on cloud amount or the "lifetime effect" (Albrecht, 1989) via precipitation modifications. Precipitation susceptibility, i.e., $S_o = -\mathrm{d}\ln R/\mathrm{d}\ln N_d$, where R is the precipitation rate and N_d is the droplet number concentration (Feingold and Siebert, 2009; Sorooshian et al., 2009) was previously introduced as a means of quantifying this effect. An alternative definition, i.e., the susceptibility of the probability of precipitation (POP) to changes in aerosol S_{pop} has been proposed: $S_{pop} = -\mathrm{d}\ln \mathrm{POP}/\mathrm{d}\ln N_a$ (e.g., Wang et al., 2012; Terai et al., 2012) because POP is more amenable to measurement and because of the high spatial variability in R. Several studies have attempted to quantify S_{pop} or S_o using satellite remote sensing (e.g., Sorooshian et al., 2009; L'Ecuyer et al., 2009), surface remote sensing (Mann et al., 2014), and in-situ aircraft observations (Terai et al., 2012). The values vary considerably depending on several factors, e.g., the definition of precipitation susceptibility, averaging scale (Duong et al., 2011), phase of cloud lifecycle (Duong et al., 2011; Feingold et al., 2013), and aerosol loading (Feingold et al., 2013). There is disagreement in the literature not only on the values of S_{pop} and S_o but also on how they depend on important controlling parameters, such as cloud depth and LWP. While quantifying the precipitation susceptibility is not the focus of this paper, we refer to two values as guidance. The first, $S_{pop} = 0.12$ (Wang et al., 2012), was derived from satellite remote sensing data. The second, $S_o \approx 1$ (Mann et al., 2014) was calculated from surface-based remote sensing observations in the northeastern Atlantic Ocean and continental Europe.

Wang et al. (2012) proposed using measurements of S_{pop} as a means of constraining LWP responses to aerosol changes in a climate model. The authors used a series

ACPD
14, 13233–13269, 2014

of climate model simulations with the NCAR Community Atmosphere Model version 5 (CAM5) and the ECHAM5-HAM2 to derive an approximate linear relationship between $\lambda = \mathrm{d}\ln\mathrm{LWP}/\mathrm{d}\ln N_a$ and S_{pop} with an intercept at approximately (0,0). Interestingly, the model output from the Multiscale Modeling Framework (MMF) version of CAM5, which resolves clouds and precipitation more reliably than the standard CAM5, also conforms to this linear relationship. The constraint on λ proceeds as follows. The output from a series of GCM simulations is used to define $\lambda = f(S_{pop})$; then, a measurement of S_{pop} combined with the model-derived $f(S_{pop})$ yields an observational constraint on λ. Wang et al. (2012) showed that because $f(S_{pop})$ has an intercept at nearly (0,0) and the measured S_{pop} is small, it follows that λ, which is the cloud LWP adjustment portion of of ERFaci, is also small. However, the authors did concede that more work must be performed to test these relationships in higher resolution models. The current work directly addresses this point. Specifically, this study addresses the generality and scale dependence of the $\lambda - S_{pop}$ relationship. The $\lambda - S_{pop}$ relationship is examined at the cloud scale based on previously published work and more rigorously via an analysis of large eddy simulation (LES) results for warm (liquid phase only) cloud systems. Observations of S_{pop} and S_o are then used to provide LES constraints on λ; the implications for albedo susceptibility (Platnick and Twomey, 1994) are also explored.

The remainder of the paper is organized as follows. Section 2 introduces the methods used to evaluate λ based on both extant literature and LES. The primary results are presented and discussed in Sect. 3. Finally, the important conclusions of this work are enumerated in Sect. 4.

2 Methods

2.1 Analysis of extant literature

If indeed the relationship between λ and S_{pop} (or S_o) is robust, one might expect this to emerge in extant literature. We therefore conducted a survey of published results from

ACPD
14, 13233–13269, 2014

a wide range of studies that simulated cases based on various field campaigns. The details of these studies are listed in Table 1. The choice of S_o vs. S_{pop} in the review of the existing literature was based on the lack of information regarding the rain fraction (or POP) in previously published studies. The potential effect of this substitution is discussed later.

2.2 LES simulations

Two different cloud regimes were explored: (i) stratocumulus, based on the Second Dynamics and Chemistry of Marine Stratocumulus (DYCOMS-II) Research Flight 2 (RF02) and (ii) trade-wind cumulus, based on the Rain in Cumulus over the Ocean (RICO) field experiment. The two different warm cloud regimes provide the opportunity to explore the robustness of both the $\lambda - S_{pop}$ and $\lambda - S_o$ relationships.

2.2.1 Stratocumulus clouds: DYCOMS-II, RF02

A suite of 25 simulations is performed with the Weather Research and Forecasting (WRF) model to explicitly examine the relationships between λ and S_{pop} and between λ and S_o. For the purposes of this study, WRF is coupled with a two-moment, bin-emulating microphysical model that has been widely used to examine aerosol-cloud interactions (Feingold et al., 1998; Wang and Feingold, 2009a). The simulations comprise 5 different initial aerosol number concentrations (i.e., $N_a = 25$, 50, 75, 100, and 125 mg^{-1}). Note that N_a is used interchangeably in this paper to denote both the aerosol number concentration (units of cm^{-3}) and mixing ratio (units of mg^{-1}) because the simulations use different initialization routines. However, because the air density is approximately 1 $kg\,m^{-3}$ for the considered domains, 1 $mg^{-1} \approx 1\ cm^{-3}$. While the aerosol concentration is a prognostic variable, the shape of the distribution is invariant with time and assumed to be lognormal with a median radius of 0.2 µm and a geometric standard deviation of 1.5. The aerosol is assumed to be composed of ammonium sulfate. Supersaturation is calculated and prognostically treated in the model; droplets are formed on

ACPD
14, 13233–13269, 2014

the aerosol particles with radii above the critical supersaturation required for activation following Köhler theory. The activated aerosol particles are removed from the aerosol population. Particles are regenerated upon evaporation of droplets assuming that one drop regenerates one aerosol particle (Mitra et al., 1992). Thus, collision-coalescence and surface rain effectively reduce the aerosol concentration.

For each N_a, a control simulation is performed based on DYCOMS-II RF02, which readily produced drizzle (Stevens et al., 2003). The WRF-LES setup described by Yamaguchi and Feingold (2012) is used. Four additional simulations are performed to explore the sensitivity to environmental conditions and microphysical process rates, i.e., increased surface latent heat flux (140 W m^{-2}, Hi-LHF), decrease surface latent heat flux (46.5 W m^{-2}, Lo-LHF), increased collision-coalescence rate (110 % of the predicted rate, Hi-CC), and decreased collision-coalescence rate (80 % of the predicted rate, Lo-CC).

All simulations are performed with a horizontal grid spacing of 50 m and a vertical grid spacing of 12 m. The domain is 6.4 km by 6.4 km in the horizontal and 1.5 km in the vertical direction. A time step of 0.2 s is used to ensure numerical stability and convergence (see Yamaguchi and Feingold, 2012). The total simulation time is 6 h; however, the initial 1 h of all simulations is discarded to allow sufficient time for turbulence to develop. The rapid radiative transfer model (RRTM) is used to calculate the longwave radiative fluxes. The simulations are assumed to be nocturnal, i.e., shortwave radiative fluxes were not included. The necessary model information is recorded at 1 min intervals, yielding nearly 5 million x, y pairs for each simulation. Although the decorrelation time for cloud fields has been shown to be much longer than 1 min (e.g., $\approx$ 15 min according to McComiskey et al., 2009), the 1 min resolution is necessary to ensure that the rare, high precipitation rate events are captured in the model output.

2.2.2 Trade-wind cumulus: RICO

The RICO simulations used in this study are adopted from Jiang et al. (2010). These simulations were performed using the Regional Atmospheric Modeling System

ACPD
14, 13233–13269, 2014

(RAMS) version 6.0 with an explicit bin-resolving microphysics scheme (Feingold et al., 1996; Stevens et al., 1996). The aerosol treatment in these simulations is very similar to that of the stratocumulus simulations (see Sect. 2.2.1). The domain size is 25.6 km × 25.6 km × 6 km with a horizontal grid spacing of 100 m and vertical grid spacing of 40 m. The Global Energy and Water Cycle Experiment Cloud System (GCSS) boundary layer working group initial sounding is modified to initiate heavier rainfall by increasing the ambient water vapor mixing ratio and decreasing the potential temperature above 1 km. The model top is also extended in Jiang et al. (2010) to 6 km to allow for deeper convection. The simulations are performed for 8 h with 5 different aerosol loadings, namely, 100, 200, 300, 400, and 500 cm^{-3}. It is important to note that even with these modifications, the sounding used still resembles the observed sounding on 19 January 2005, during the RICO campaign. As in the case of the stratocumulus simulations, model output at 1 min intervals is used. For additional information on these simulations, the reader is referred to Jiang et al. (2010).

2.3 λ calculation

The LWP was first calculated for every column and for every output time by including only cloud water, which is consistent with the method used in Wang et al. (2012). Here, λ is approximated as follows:

$$\lambda = \frac{\mathrm{d}\ln \mathrm{LWP}}{\mathrm{d}\ln N_\mathrm{a}} \approx \frac{\Delta \ln \mathrm{LWP}}{\Delta \ln N_\mathrm{a}} = \left\langle \frac{\ln \overline{\mathrm{LWP}^{(2)}} - \ln \overline{\mathrm{LWP}^{(1)}}}{\ln N_\mathrm{a}^{(2)} - \ln N_\mathrm{a}^{(1)}} \right\rangle, \quad (1)$$

where the overbars represent spatial (horizontal) means and the brackets represent temporal means. The superscripts correspond to low (1) and high (2) aerosol loading scenarios. The results were found to be qualitatively (and nearly quantitatively) insensitive to the order in which the calculations were performed, i.e., taking the temporal average of the relative differences (as in Eq. 1) or taking the relative difference of the temporal averages.

ACPD
14, 13233–13269, 2014

2.4 S_{pop} calculation

To calculate S_{pop}, we first determined if it was raining at the surface in a given grid cell and assigned the grid cell a probability of $P = 1$ if it was raining and $P = 0$ otherwise – namely, the precipitation probability $P(t)$ as a function of time t is conditional on a threshold rain rate T_h:

$$P_{i,j}^{(k)}(t) = \begin{cases} 1 & \text{if } R_{i,j}^{(k)}(t) \geq T_h \\ 0 & \text{if } R_{i,j}^{(k)}(t) < T_h \end{cases} \quad (2)$$

where T_h represents a predefined threshold in mm day^{-1} and the superscript k corresponds to the specific simulation. The surface rain rate was used for the calculations herein. Then, S_{pop} was calculated similar to λ, i.e.,

$$S_{pop} = -\frac{d\ln POP}{d\ln N_a} \approx -\frac{\Delta \ln POP}{\Delta \ln N_a} = -\left\langle \frac{\ln \overline{P^{(2)}} - \ln \overline{P^{(1)}}}{\ln N_a^{(2)} - \ln N_a^{(1)}} \right\rangle. \quad (3)$$

For calculating P, 10 thresholds were applied to R, ranging from 10^{-6} to 20 mm day^{-1}. Only a representative subset of these calculations is presented in this paper.

2.5 S_o calculation

Here, S_o was computed by conditionally averaging the rain rate over the aforementioned rain rate thresholds. However, in keeping with Feingold and Siebert (2009), the denominator is $d\ln N_d$ instead of $d\ln N_a$; therefore, we have

$$S_o = -\frac{d\ln R}{d\ln N_d} \approx -\frac{\Delta \ln R}{\Delta \ln N_d} = -\left\langle \frac{\ln \overline{R^{(2)}} - \ln \overline{R^{(1)}}}{\ln \overline{N_d^{(2)}} - \ln \overline{N_d^{(1)}}} \right\rangle, \quad (4)$$

where all of the variables and symbols are defined above.

ACPD
14, 13233–13269, 2014

2.6 $S_{o,\,mod}$ and $S_{pop,\,mod}$ calculations

Two additional parameters were computed, i.e., $S_{o,\,mod}$ and $S_{pop,\,mod}$; $S_{o,\,mod}$ is the same as in Eq. (4) except that N_a replaces N_d in the denominator. Similarly, $S_{pop,\,mod}$ replaces N_a with N_d in the denominator of Eq. (3). These modified parameters are useful for analyzing the sensitivity of the results to the use of N_a or N_d, in which the latter evolves with time and the former is used to represent the response in the system to an initial change in aerosol loading, which is similar to the approach used in global climate simulations. The simulations also help to examine the robustness of results to multiple representations of precipitation susceptibility.

2.7 A_f calculations

While values of λ constrained by $f(S_{pop})$ and/or $f(S_{o,\,mod})$ are far from certain, the estimates provided herein for the different cloud regimes can be used to estimate the potential effects of changes in aerosol loading on albedo susceptibility A'_o. We begin with the definition of A'_o from Feingold and Siebert (2009):

$$A'_o = A_o \left[1 + \frac{5}{2}\frac{d\ln LWP}{d\ln N_d} + \ldots\right], \quad (5)$$

where A_o represents the albedo susceptibility under constant LWP conditions, i.e.,

$$A_o = \left.\frac{d\ln A}{d\ln N_d}\right|_{LWP} = \frac{1-A}{3}, \quad (6)$$

and all other terms have been previously defined. The ellipsis on the right hand side of Eq. (5) represents additional terms that have been excluded in this study. These terms can include such effects as changes in the breadth of the drop size distribution (Feingold and Siebert, 2009). However, Eq. (5) is provided in terms of incremental changes in N_d, whereas, the LWP susceptibility, i.e., λ, is defined relative to incremental

ACPD
14, 13233–13269, 2014

changes in N_a. Therefore, we make use of a power law relationship between N_d and N_a:

$$N_d \propto N_a^c, \tag{7}$$

where c is theoretically ≤ 1. Previous studies have provided a broad range of values for c. For example, Shao and Liu (2009) suggested a range of 0.25 to 0.85 based on direct measurements of both polluted and clean clouds. Other studies have shown that c is likely on the higher end of this range in relatively clean conditions, i.e., $N_a < 500\,\mathrm{cm}^{-3}$ (e.g. Conant et al., 2004; Twohy et al., 2005). Therefore, we chose a characteristic value of 0.75 (or 3/4) for c in this study. As a result, the relationship presented in Eq. (7) can be rewritten as

$$\frac{\mathrm{d}\ln N_d}{\mathrm{d}\ln N_a} = c = \frac{3}{4}. \tag{8}$$

Then, by rewriting Eq. (5) as

$$A_o' = A_o\left[1 + \frac{5}{2}\frac{\mathrm{d}\ln \mathrm{LWP}}{\mathrm{d}\ln N_a}\frac{\mathrm{d}\ln N_a}{\mathrm{d}\ln N_d} + \ldots\right], \tag{9}$$

and incorporating Eq. (8), we get

$$A_o' = A_o\left[1 + \frac{10}{3}\lambda + \ldots\right]. \tag{10}$$

Because we are not necessarily concerned here with the specific values of either A_o' or A_o, we define the albedo susceptibility enrichment factor A_f as follows:

$$A_f = \frac{A_o'}{A_o} = \left[1 + \frac{10}{3}\lambda + \ldots\right]. \tag{11}$$

ACPD
14, 13233–13269, 2014

Thus $\lambda = 0.3$ corresponds to a doubling of the albedo susceptibility relative to the value under constant LWP conditions. Calculations of A_f using Eq. (1) will be shown alongside those of λ for the two cloud types. Previous studies have provided estimates of both S_{pop} (0.12, Wang et al., 2012) and $S_{o,\,mod}$ (0.66, Mann et al., 2014) using satellite-based and ground-based observations, respectively. Mann et al. (2014) reported the precipitation susceptibility in terms of incremental changes in N_a, which corresponds to $S_{o,\,mod}$ in this study. However, precipitation susceptibility has been previously defined in numerous studies relative to incremental changes in N_d (i.e., S_o). Therefore, using Eq. (8), one finds that S_o is nearly 1.

3 Results

3.1 Analysis of extant literature

An initial review of the literature revealed several interesting components relevant to understanding the relationship between λ and S_{pop} (or S_o). First, the lack of detailed information regarding the rain fraction or POP made it impossible to determine accurate values of S_{pop} from previously published results. Therefore, we chose to use S_o in our analysis of the published literature. However, even with this assumption, several studies still lacked the necessary details to determine a relationship between λ and S_o due to either the lack of information regarding N_d (needed to calculate S_o) or the lack of information regarding the initial aerosol number concentration (needed to calculate λ). As a result, we show the findings from the published literature in Fig. 1 for λ' as a function of S_o', where the "prime" denotes that the axes are not necessarily the same for *all* points. Specifically, S_o' is $\mathrm{d}\ln R/\mathrm{d}\ln N_a$ in Jiang et al. (2010) and λ' is $\mathrm{d}\ln \mathrm{LWP}/\mathrm{d}\ln N_d$ in Berner et al. (2011). For all other references, $\lambda' = \lambda$ and $S_o' = S_o$, as defined in Eqs. (1) and (4), respectively.

Furthermore, because the model output was unavailable from many of these studies, every effort was made to carefully read off the relevant values of LWP, R and N_a (or

ACPD
14, 13233–13269, 2014

a similar aerosol measurement, such as the number concentration of cloud condensation nuclei N_{CCN} or N_d) from the published figures. Although a consistent methodology was applied to calculate λ' and S'_o, we make no claims on the accuracy of these results. The main point is to see whether any trends in λ' vs. S'_o emanate from different models and for different environmental conditions. Figure 1 shows substantial variability in the λ'–S'_o relationship. Depending upon which subset of points are selected, one can find a negative slope (e.g., green squares Wang and Feingold, 2009a), nearly no slope (e.g., red closed circles, Berner et al., 2011), and a positive slope (e.g., blue crosses, Wang and Feingold, 2009a). Interestingly, Wang and Feingold (2009a) suggests either a positive or a negative slope, depending upon how the LWP and R are averaged over the domain (i.e., averaging all of the grid points or conditionally averaging grid points that exceed some predefined threshold). Regardless, none of the slopes predicted by the individual studies exhibits an intercept near (0,0). Moreover, the slopes of these lines tend to be negative or nearly 0, unlike the coarser grained climate model results in Wang et al. (2012). A more in-depth analysis is clearly warranted.

3.2 Stratocumulus LES (DYCOMS-II)

3.2.1 Rain rates

The LES results are presented below in the context of three specific thresholds on R. These thresholds are utilized to mimic minimum detectable limits for R from current satellite-based retrievals (and potentially from future satellite platforms). The three values for T_h are 0.001, 0.5, and 5 mm day^{-1}. For perspective, the minimum detectable radar reflectivity for CloudSat is −30 dBZ (e.g., Haynes et al., 2009), while the minimum for the Tropical Rainfall Measuring Mission (TRMM) is 17 dBZ. These reflectivities roughly correspond to precipitation rates of 0.5 and 5 mm day^{-1}, respectively. While inherent uncertainties in the Z–R relationships (emanating from, e.g., assumed drop size distributions and attenuation) can contribute to small variations in the lowest

ACPD
14, 13233–13269, 2014

detectable rain rates. we use T_h of 0.5 and 5 mm day^{-1} to represent of CloudSat and TRMM precipitation rate observations, respectively.

Before delving into the relative changes in LWP, R, and POP, it is necessary to first evaluate the absolute range of R produced in the simulations. Figure 2 depicts the mean (solid) and median (dashed) rain rates for T_h of 0.001 (gray), 0.5 (blue), and 5 (red) mm day^{-1} for the DYCOMS-II simulations. The shaded area encompasses the 10th to the 90th percentiles. Figure 2a shows that the average R is approximately 1–2 mm day^{-1} for T_h of 0.001 and 0.5 mm day^{-1} and $N_a = 25$ mg^{-1}; the 90th percentile approaches 10 mm day^{-1}. The values decrease as N_a increases (Fig. 2b–d).

In general, there is a small increase in the mean and median R as T_h increases from 0.001 to 0.5 mm day^{-1}. However, the increase is much more substantial for a further increase in T_h to 5 mm day^{-1}. At this high threshold, the mean R is nearly equivalent to the 90th percentile for T_h of 0.001 and 0.5 mm day^{-1}; therefore, most of the lightly drizzling grid points are excluded by choosing such a high T_h. The importance of these thresholds on R will be discussed in more detail below with respect to incremental increases in N_a. Figure 2 excludes the model results for $N_a = 125$ mg^{-1} because R was too small for all but the smallest T_h to be confident in the averaged values of POP and R.

3.2.2 λ–S_{pop} Relationship and A_f

It is important to note that for ease in interpretation of the LES results, we present the analysis of the 25 DYCOMS-II simulations (and the 5 RICO simulations presented below) using S_{pop}, which is identical to S_{pop} in Wang et al. (2012) except that the aerosol index (AI; the product of the Ångstrom coefficient and the aerosol optical depth) is replaced with N_a, i.e., the initial aerosol concentration that was used in the simulations. This change should have little if any effect on the qualitative nature of the findings presented here given the nearly linear relationship observed between the AI and N_a or N_{CCN} (e.g. Nakajima et al., 2001; Liu and Li, 2014).

ACPD
14, 13233–13269, 2014

Figure 4 suggests several important results. First, the relationship between λ and S_{pop} depends on the chosen R threshold (i.e., T_h). The λ–S_{pop} slope tends to decrease as T_h increases, especially when only examining relatively small changes in N_a (i.e., black and red points). In fact, for $T_h = 0.001$ mm day^{-1}, $S_{pop} \simeq 0$ for a change in N_a from 25 mg^{-1} to 50 mg^{-1}. In those relatively clean conditions, with such a low T_h, nearly all grid points are precipitating; a small absolute change in N_a is not sufficient to decrease R such that R becomes less than T_h for a substantial subset of the domain; hence, little if any change is found in POP in response to increases in N_a. This finding suggests that for low T_h, POP may be largely insensitive to changes in N_a in relatively clean environments, especially for these stratocumulus simulations. However, for higher T_h, even in relatively clean conditions, a doubling of N_a produces an increase in S_{pop} (Fig. 4c) because in these conditions, even a change in N_a from 25 mg^{-1} to 50 mg^{-1} is sufficient to reduce R such that R becomes less than $T_h = 5$ mm day^{-1} for a substantial subset of the domain.

Furthermore, Fig. 4a suggests that for marine stratocumulus λ likely does not increase indefinitely as S_{pop} increases. Instead, an asymptotic behavior is suggested whereby any further increase in S_{pop} produces a smaller or nearly no change in λ. It is at this point that the change in N_a is sufficiently large to permit aerosol-induced evaporation-entrainment or sedimentation-entrainment effects to play a role. In other words, further suppression in POP does not lead to an additional increase in LWP because the much smaller droplets are more readily evaporated (e.g., Wang et al., 2003; Ackerman et al., 2004; Xue and Feingold, 2006) or because weaker sedimentation enhances both evaporation and cloud-top cooling, both of which increase entrainment (Bretherton et al., 2007). This asymptotic behavior is challenging to discern for higher T_h due to an insufficient number of points for which R exceeds T_h in the presence of higher aerosol loadings. However, the inability for λ to increase indefinitely as POP is further reduced should be expected given previously published findings. For example, Ackerman et al. (2004) demonstrated that LWP first increases with increasing N_a ($\lambda > 0$), however further increases in N_a result in $\lambda = 0$. Ultimately, for a strong

ACPD
14, 13233–13269, 2014

enough aerosol perturbation, λ becomes negative; however, under these conditions clouds are likely not precipitating and λ is dominated by processes other than collision-coalescence.

As mentioned above, $T_h = 0.5\,\mathrm{mm\,day^{-1}}$ corresponds roughly to the threshold that is commonly used to determine precipitating locations in the CloudSAT dataset. However, the results presented in Fig. 4 suggest that such a threshold may not be capable of capturing the entire parameter space for the selected case. Furthermore, such a large threshold tends to suppress the LWP response to changes in N_a (i.e., λ), i.e., the intercept approaches (0,0) as $T_h \longrightarrow 5\,\mathrm{mm\,day^{-1}}$ for these stratocumulus clouds. Physically, an intercept of ≈ 0 seems unlikely. Hypothetically, if an increase in N_a results in no change in POP ($S_{pop} = 0$), the LWP should increase as the cloud droplets become smaller and more numerous and rain formation becomes less efficient. Therefore, in readily precipitating clouds, one would expect that the LWP should increase in response to increasing N_a ($\lambda > 0$), as suggested in Fig. 4a and b. Both observational studies (Christensen and Stephens, 2011) and LES (e.g., Wang et al., 2003; Ackerman et al., 2004; Xue et al., 2008) have confirmed $\lambda > 0$ for readily precipitating clouds. However, λ can become negative in the presence of high aerosol loadings and readily precipitating cloud (discussed below with regard to the RICO simulations). Regardless, the high-resolution LES results for stratocumulus clouds presented herein suggest that for $S_{pop} = 0.12$ (Wang et al., 2012), λ varies between nearly 0 for high T_h to approximately 0.5 for lower T_h.

Figure 4 also provides a useful estimate of A_f for marine stratocumulus by applying Eq. (11) to the simulated values of λ. The right axes of the plots in Fig. 4 demonstrate the range of possible A_f. For a value of S_{pop} of 0.12 or by simply choosing the results for small changes in N_a, the DYCOMS-II RF02 simulations suggest that A_f is between 1.8 and 2.5, i.e., the albedo susceptibly may be 80 % to 150 % higher than expected under constant LWP conditions.

ACPD
14, 13233–13269, 2014

3.2.3 λ–$S_{pop,\,mod}$ relationship

Fig. 5 shows the relationship between λ and $S_{pop,\,mod}$, in which the denominators of the x and y axes are no longer identical. For low T_h, changing the denominator has little to no effect on the relationship between relative changes in LWP and POP (Fig. 5a). However, for higher T_h, i.e., values that better reflect the lower detection limits of satellite retrievals, the inconsistent denominator causes the relationship to become less linear and more chaotic, especially for $T_h = 5\,\mathrm{mm\,day^{-1}}$. The reason for this discrepancy is related to the fact that the relative changes in LWP and POP due to changes in N_a reflect a response due to the prescribed aerosol perturbation, i.e., the changes are relative to only the initial aerosol loading, whereas relative changes in LWP and POP due to changes in N_d reflect the effects of numerous microphysical processes (e.g., activation, collision-coalescence, and scavenging). Because N_d is not constant in time, the relative change in N_d tends to vary as a function of time. This transient nature produces the chaotic behavior in Fig. 5b and c.

3.2.4 λ–$S_{o,\,mod}$ relationship and A_f

As discussed above, S_o is typically represented in terms of relative changes in N_d. However, the previous subsection demonstrated how inconsistencies in the denominator can cause the relationship between λ and S_{pop} to become chaotic and no longer exhibit a clear trend. Therefore, we show the relationship between λ and $S_{o,\,mod}$, i.e., where the denominators in the x and y axes are both a function of the relative change in N_a (Fig. 6). As mentioned in Sect. 3.2.2, small changes in N_a exhibit little to no effect on POP when a low threshold on R is applied to determine raining and non-raining locations. However, the same does not hold true for R, i.e., even at low thresholds, R still changes due to increases in aerosol loading, even for small absolute changes. Therefore, the stratocumulus clouds continue to precipitate throughout most of domain for imposed increases in N_a, yet the average R is slightly reduced. This effect is

ACPD
14, 13233–13269, 2014

demonstrated in Fig. 6a, where we see that $S_{o,\,mod}$ is greater than 0 (unlike the case for S_{pop}, Fig. 4a).

A comparison between Figs. 4 and 6 suggests that the relationships are qualitatively the same (i.e., λ tends to increase as either S_{pop} or $S_{o,\,mod}$ increases), although the slopes can be quite different. The difference in slopes is related to the aforementioned point about how changes in N_a act differently on R and POP. In the case of $S_{o,\,mod}$, small changes in N_a do little to affect the average R in the heavily drizzling regions, i.e., the high threshold is inclusive enough to maintain a relatively constant average R for all aerosol perturbations. On the other hand, for low T_h, nearly the entire domain is considered to be drizzling and a small change in N_a reduces R. However, because this reduction is not sufficient to convert many drizzling locations into non-drizzling points, S_o increases (Fig. 6a) while S_{pop} (Fig. 4a) remains nearly constant for small changes in N_a.

Using the $S_{o,\,mod} = 0.66$ observational constraint from Mann et al. (2014) (note that $S_o \approx 1$ for realistic values of c) for this scenario, one arrives at values of λ ranging from 0.4 to 1.0 for $T_h = 0.001\,mm\,day^{-1}$ and $T_h = 0.5\,mm\,day^{-1}$, respectively. For $T_h = 5\,mm\,day^{-1}$, Fig. 6c suggests that λ would be substantially larger; however, the simulations do not extend to large enough N_a to quantify this effect. The right hand axes of Fig. 6 provide equivalent estimates of A_f derived from Eq. (11) and point to enhancements in the albedo susceptibility of 2.5 (4) for $T_h = 0.001\,mm\,day^{-1}$ ($0.5\,mm\,day^{-1}$).

3.3 Trade-wind cumulus: RICO LES

3.3.1 Rain rates

Figure 3a shows that the average R for $N_a = 100\,cm^{-3}$ is approximately 10–$20\,mm\,day^{-1}$ for T_h of 0.001 and $0.5\,mm\,day^{-1}$ in the simulated trade-wind clouds (the domain average is naturally much less than this, however the threshold removes very small values of R such that the average R is higher). The average R for all thresholds

ACPD
14, 13233–13269, 2014

tends to decrease as N_a increases (Fig. 3b–e); the largest change occurs when N_a increases from 300 to 400 cm^{-3} (Fig. 3c and d). The changes in R for increasing N_a are similar to those shown for the stratocumulus case (Fig. 2) except that R tends to change more rapidly in the trade-wind cumulus, especially for higher aerosol loadings. Moreover, Fig. 3 demonstrates that the clouds precipitate for all aerosol loading scenarios and under all threshold values in the RICO case; therefore, the analysis that follows incorporates all 5 RICO simulations.

3.3.2 λ–S_{pop}, $S_{pop,\,mod}$, and $S_{o,\,mod}$ relationships and A_f

The RICO simulations elicit an important finding that was alluded to earlier. Namely, λ is not necessarily positive. Figure 7 demonstrates that λ is negative for changes in N_a that are a factor of 3 or larger. Moreover, Fig. 7a suggests that in the case of these shallow trade-wind cumulus clouds, λ does not increase as S_{pop} increases; in fact, the opposite is true. This downward trend is related to the balance between aerosol perturbations acting to decrease R, and to increase entrainment and evaporation within the cloud. The former acts to increase S_{pop}, while the latter decreases λ. However, the simulations also suggest that λ saturates, which was suggested earlier in the case of stratocumulus clouds (Fig. 4). For larger and larger changes in N_a, S_{pop} continues to increase while λ remains relatively constant. This asymptotic behavior is because the changes in droplet size for increases in aerosol loading beyond 400 cm^{-3} are smaller relative to an increase in N_a from 100 to 200 mg^{-1} and thus limit additional evaporation-entrainment feedbacks on the cloud system. This is analogous to the findings of Xue and Feingold (2006) (Figs. 3 and 5 therein), who showed that several cloud characteristics (e.g., LWP and cloud fraction) asymptote for high aerosol number concentrations. This effect is largely related to the system converging on the saturation adjustment limit, which suppresses further decreases in λ. The results of the RICO simulations for small changes in N_a (i.e., from 100 to 200 cm^{-3}) suggest that A_f may be similar for both marine stratocumulus and trade-wind cumulus (i.e., approximately 1.7 for the RICO simulations). However, whereas A_f was shown to increase for larger changes in N_a in

ACPD
14, 13233–13269, 2014

marine stratocumulus (Fig. 4), A_f tends to decrease in the case of trade-wind cumulus. In this case, the LWP response to an aerosol perturbation acts to *decrease* the albedo susceptibility (A_f is less than 1).

The DYCOMS-II stratocumulus simulations demonstrated that the consistency in the denominator of the x- and y-axes was important for predicting an increase in λ as a function of S_{pop} or $S_{o,\,mod}$. However, in the trade-wind cumulus case, this effect is not seen (Figs. 7a and b are very similar). This follows because an increase in N_a results in an increase in N_d that does not vary much over the course of the 8 h simulations (Fig. 8a). This was not true in the case of drizzling stratocumulus clouds, where N_d decreased with time (Fig. 8b). Therefore, in the stratocumulus simulations, the relative droplet number concentration increases, especially when comparing the pristine simulation ($N_a = 25\,mg^{-1}$) with the more polluted cases (i.e., $N_a = 100$ and $125\,mg^{-1}$). We suggest that the difference is related to the different cloud systems. In the case of trade-wind cumulus, only a small fraction of the domain contains cloud water at any given time; therefore the time required to scavenge a large portion of the ambient aerosol is much longer than in the case of stratocumulus clouds where the cloud fraction is often nearly 1. This effect is demonstrated in Fig. 8, where the increase in the relative droplet number concentration (i.e., $N_d/N_{d,0}$) for the larger aerosol perturbations in the stratocumulus scenario corresponds to the rapid decrease in N_d in the low aerosol loading case as a result of the efficient removal of aerosol from the domain.

Furthermore, Fig. 7a and b suggest that λ decreases more rapidly with increased aerosol loading for lower T_h. For $T_h = 0.001\,mm\,day^{-1}$, λ decreases from approximately 0.2 to −0.8 for an increase in S_{pop} of only 0.8. However, for $T_h = 5\,mm\,day^{-1}$, λ decreases from approximately 0.2 to −0.8 for an increase in S_{pop} of 2.5. This has important implications for constraining λ using observations of S_{pop}. For example, if the former trend is true, then small values of S_{pop} result in small values of λ, as suggested by Wang et al. (2012). However, if the latter trend is true, i.e., λ decreases gradually with increasing N_a (and increasing S_{pop}), then a small value of S_{pop} implies a larger λ. For reference, if S_{pop} is 0.12 (Wang et al., 2012), then λ is approximately 0 for

ACPD
14, 13233–13269, 2014

$T_h = 0.001\,\mathrm{mm\,day^{-1}}$ (Fig. 7a, closed circles), while λ increases to approximately 0.3 for $T_h = 5\,\mathrm{mm\,day^{-1}}$ (determined by extrapolating the points to smaller values of S_{pop} in Fig. 7a, diamonds). Alternatively, if $S_{o,\,mod} = 0.66$ (Mann et al., 2014), then Fig. 7c indicates that λ ranges from 0.3 ($T_h = 0.001\,\mathrm{mm\,day^{-1}}$) down to 0.05 ($T_h = 5\,\mathrm{mm\,day^{-1}}$). Therefore, the equivalent range of A_f range is an enhancement of 20 % to 100 % relative to constant LWP conditions. However, for even slightly higher $S_{o,\,mod}$, λ quickly becomes negative and A_f becomes less than 1.

4 Conclusions

Wang et al. (2012) explored the relationship between the LWP response to an increase in aerosol loading λ and the precipitation frequency susceptibility S_{pop} in climate model simulations. If a robust relationship between λ and S_{pop} were to exist, observations of S_{pop} would provide a strong constraint on λ in climate studies. The current work examines this relationship at the large eddy scale.

First, a review of the literature suggests that the relationship between λ and S_o need not be positive nor linear; however, these results exhibited little quantitive power given the paucity of the model output from the previous studies. To explore this relationship in more detail, a set of large eddy simulations of a drizzling stratocumulus case was performed, and a previously published set of trade-wind cumulus simulations was analyzed. In each of these sets, the simulations differ only in their initial aerosol concentration, allowing us to explore albedo susceptibility in an idealized framework.

The following important findings were drawn from this analysis. Although they are formulated with respect to S_{pop} for brevity, these conclusions apply more generally to $S_{o,\,mod}$ as well.

1. The y-intercept of the λ–S_{pop} relationship is likely > 0, for both stratocumulus and trade-wind cloud systems. This differs from the climate-model derived intercept of 0 in Wang et al. (2012)

ACPD
14, 13233–13269, 2014

2. λ does not necessarily increase linearly as a function of S_{pop}. Instead, λ exhibits an asymptotic behavior at sufficiently large S_{pop}. In the case of stratocumulus, aerosol-induced evaporation-entrainment and/or sedimentation-entrainment effects limit further increases in the LWP. This effect is schematically represented in Fig. 9 (red, stippled). For trade-wind cumulus clouds, λ is shown to *decrease* with increasing S_{pop} due to the effects of entrainment and evaporation (Fig. 9; blue, dotted). These different trends in λ are important if one wishes to diagnose λ from observations of S_{pop} or $S_{o,\,mod}$, especially for small aerosol perturbations, which are reflected by larger changes in λ and small changes in both S_{pop} (Fig. 9; crossed).

3. At the $S_{pop} = 0$ intercept, λ is approximately 0.2–0.3 in both the stratocumulus and trade-wind cumulus. However, the simulations suggest that λ may increase or decrease with increased aerosol loading (and increasing S_{pop}) depending on the cloud type and dominant microphysical processes. Specifically, the results presented herein suggest that λ increases in marine stratocumulus and decreases in the case of trade-wind cumulus (Fig. 9).

4. To gauge the influence of these results on albedo susceptibility, we calculated A_f, the fractional enhancement in the albedo susceptibility relative to constant LWP conditions. For the stratocumulus cloud case, A_f ranges from enhancements of 80 % to 150 % if $S_{pop} = 0.12$ (Wang et al., 2012) is used as a constraint or approximately 150 % to 300 % if $S_{o,\,mod} = 0.66$ (Mann et al., 2014) is the constraint. Moreover, in the case of the trade-wind cumulus clouds, the A_f ranges are 20–80 % for $S_{pop} = 0.12$ and 70 % for $S_{o,\,mod} = 0.66$. However, for slightly higher S_{pop} or $S_{o,\,mod}$, the albedo susceptibility may actually decrease relative to constant LWP conditions due to the strong leverage of λ in Eq. (11).

5. The importance of using a consistent denominator in the λ and S_{pop} calculations was demonstrated by calculating S_{pop} (but not λ) in terms of N_d rather than N_a (i.e., $S_{pop,\,mod}$). The introduced inconsistency is important in the case of stratocumulus

ACPD
14, 13233–13269, 2014

clouds in which N_d decreases (quite rapidly in relatively clean conditions) as a function of time. This effect produces an ill-defined relationship between λ and $S_{pop,\,mod}$.

In general, while a measurement of S_{pop} is practical from a remote-sensing stand point and the use of a GCM allows for the analysis of the entire climate system, the λ–S_{pop} relationship is likely related to the resolution of convection, the scales at which the aerosol interacts with clouds, and the type of system (i.e., stratocumulus vs. trade-wind cumulus). Based on our earlier work (McComiskey and Feingold, 2012), we surmise that even if convection and aerosol-cloud processes are adequately resolved, the λ–S_{pop} relationship will also be dependent on the scale at which data are aggregated. Determining POP is a binary option, i.e., it is either raining or it is not, which is dependent on some threshold for what is considered "raining". It has been shown here that the slope and intercept of the λ–S_{pop} is largely dependent upon the selected rain threshold. We therefore caution that these scale, threshold, and aerosol proxy sensitivities be carefully considered before λ–S_{pop} relationships are universally applied.

Acknowledgements. The authors thank the Department of Energy's Atmospheric System Research Program and NOAA's Climate Goal for funding. Hongli Jiang is thanked for providing the RICO simulations.

References

Ackerman, A. S., Toon, O. B., and Hobbs, P. V.: A model for particle microphysics, turbulent mixing, and radiative transfer in the stratocumulus-topped marine boundary layer and comparisons with measurements, J. Atmos. Sci., 52, 1204–1236, 1995. 13260

Ackerman, A. S., Kirkpatrick, M. P., Stevens, D. E., and Toon, O. B.: The impact of humidity above stratiform clouds on indirect aerosol climate forcing, Nature, 432, 1014–1017, 2004. 13246, 13247, 13260

Albrecht, B.: Aerosols, cloud microphysics, and fractional cloudiness, Science, 245, 1227–1230, doi:10.1126/science.245.4923.1227, 1989. 13235

ACPD
14, 13233–13269, 2014

Berner, A. H., Bretherton, C. S., and Wood, R.: Large-eddy simulation of mesoscale dynamics and entrainment around a pocket of open cells observed in VOCALS-REx RF06, Atmos. Chem. Phys., 11, 10525–10540, doi:10.5194/acp-11-10525-2011, 2011. 13243, 13244, 13260, 13261

Bréon, F., Tanré, D., and Generoso, S.: Aerosol effect on cloud droplet size monitored from satellite, Science, 295, 834–838, doi:10.1126/science.1066434, 2002. 13235

Bretherton, C. S., Blossey, P. N., and Uchida, J.: Cloud droplet sedimentation, entrainment efficiency, and subtropical stratocumulus albedo, Geophys. Res. Lett., 34, L03813, doi:10.1029/2006GL027648, 2007. 13246

Christensen, M. W. and Stephens, G. L.: Microphysical and macro physical responses of marine stratocumulus polluted by underlying ships: eevidence of cloud deepening, J. Geophys. Res., 116, D03201, doi:10.1029/2010JD014638, 2011. 13247

Conant, W. C., VanReken, T. M., Rissman, T. A., Varutbangkul, V., Jonsson, H. H., Nenes, A., Jimenez, J. L., Delia, A. E., Bahreini, R., Robets, G. C., Flagan, R. C., and Seinfeld, J. H.: Aerosol-cloud drop concentration closure in warm cumulus, J. Geophys. Res., 109, D13204, doi:10.1029/2003JD004324, 2004. 13242

Cotton, W. R., Pielke Sr., R. A., Walko, R. L., Liston, G. E., Tremback, C. J., Jiang, H., McAnelly, R. L., Harrington, J. Y., Nicholls, M. E., Carrio, G. G., and McFadden, J. P.: RAMS 2001: Current status and future directions, Meteor. Atmos. Phys., 82, 5–29, doi:10.1007/s00703-001-0584-9, 2003. 13260

Duong, H. T., Sorooshian, A., and Feingold, G.: Investigating potential biases in observed and modeled metrics of aerosol-cloud-precipitation interactions, Atmos. Chem. Phys., 11, 4027–4037, doi:10.5194/acp-11-4027-2011, 2011. 13235

Feingold, G. and Siebert, H.: Cloud-Aerosol Interactions from the micro to cloud scale, in: Clouds in the Perturbed Climate System: Their Relationship to Energy Balance, Atmospheric Dynamics, and Precipitation, edited by: Heintzenberg, J. and Charlson, R. J., MIT Press, Cambridge, MA, USA, 2009. 13235, 13240, 13241

Feingold, G., Stevens, B., Cotton, W. R., and Frisch, A. S.: The relationship between drop in-cloud residence time and drizzle production in numerically simulated stratocumulus clouds, J. Atmos. Sci., 53, 1108–1122, 1996. 13239, 13260

Feingold, G., Walko, R. L., Stevens, B., and Cotton, W. R.: Simulations of marine stratocumulus using a new microphysical parameterization scheme, Atmos. Res., 47, 505–528, 1998. 13237, 13260

ACPD
14, 13233–13269, 2014

Feingold, G., McComiskey, A., Rosenfeld, D., and Sorooshian, A.: On the relationship between cloud contact time and precipitation susceptibility to aerosol, J. Geophys. Res., 118, 10544–10554, doi:10.1002/jgrd.50819, 2013. 13235

Haynes, J. M., L'Ecuyer, T. S., Stephens, G. L., Miller, S. D., Mitrescu, C., Wood, N. B., and Tanelli, S.: Rainfall retrieval over the ocean with spaceborne W-band radar, J. Geophys. Res., 114, D00A22, doi:10.1029/2008JD009973, 2009. 13244

Jiang, H., Feingold, G., and Sorooshian, A.: Effect of aerosol on the susceptibility and efficiency of precipitation in warm trade cumulus clouds, J. Atmos. Sci., 67, 3525–3540, 2010. 13238, 13239, 13243, 13260, 13261, 13263, 13267

Khairoutdinov, M. F. and Randall, D. A.: Cloud resolving modeling of the ARM summer 1997 IOP: Model formulation, results, uncertainties, and sensitivities, J. Atmos. Sci., 60, 607–625, 2003. 13260

L'Ecuyer, T. S., Berg, W., Haynes, J., Lebsock, M., and Takemura, T.: Global observations of aerosol impacts on precipitation occurrence in warm maritime clouds, J. Geophys. Res., 114, D09211, doi:10.1029/2008JD011273, 2009. 13235

Lee, S., Feingold, G., and Chuang, P. Y.: Effect of Aerosol on CLoud-Environmental Interactions in Trade cumulus, J. Atmos. Sci., 69, 3607–3632, doi:10.1175/JAS-D-12-026.1, 2012. 13260

Liu, J. and Li, Z.: Estimation of cloud condensation nuclei concentration from aerosol optical quantities: influential factors and uncertainties, Atmos. Chem. Phys., 14, 471–483, doi:10.5194/acp-14-471-2014, 2014. 13245

Mann, J. A., Chiu, J. C., Hogan, R. J., O'Connor, E. J., L'Ecuyer, T. S., Stein, T. H. M., and Jefferson, A.: Aerosol impacts on drizzle properties in warm clouds from ARM Mobile Facility maritime and continental deployments, J. Geophys. Res., 119, 4136–4148, doi:10.1002/2013JD021339, 2014. 13235, 13243, 13249, 13252, 13266, 13267

McComiskey, A. and Feingold, G.: Quantifying error in the radiative forcing of the first aerosol indirect effect, Geophys. Res. Lett., 35, L02810, doi:10.1029/2007GL032667, 2008. 13235

McComiskey, A. and Feingold, G.: The scale problem in quantifying aerosol indirect effects, Atmos. Chem. Phys., 12, 1031–1049, doi:10.5194/acp-12-1031-2012, 2012. 13235, 13254

McComiskey, A., Feingold, G., Frisch, A. S., Turner, D. D., Miller, M. A., Chiu, J. C., Min, Q., and Ogren, J. A.: An assessment of aerosol-cloud interactions in marine stratus clouds based on surface remote sensing, J. Geophys. Res., 114, D09203, doi:10.1029/2008JD011006, 2009. 13238

ACPD
14, 13233–13269, 2014

Mitra, S. K., Brinkmann, J., and Pruppacher, H. T.: A wind tunnel study on the drop-to-particle conversion, J. Aerosol Sci., 23, 245–256, 1992. 13238

Morrison, H. and Gettelman, A.: A new two-moment bulk stratiform cloud microphysics scheme in the community atmosphere model, version 3 (CAM3), Part I: Description and numerical tests, J. Climate, 21, 3642–3659, 2008. 13260

Nakajima, T., Higurashi, A., Kawamoto, K., and Penner, J. E.: A possible correlation between satellite-derived cloud and aerosol microphysical parameters, Geophys. Res. Lett., 28, 1171–1174, 2001. 13245

Ogura, Y. and Phillips, N.: Scale analysis of deep and shallow convection in the atmosphere, J. Atmos. Sci., 19, 173–179, 1962. 13260

Platnick, S. and Twomey, S.: Determining the susceptibility of cloud albedo to changes in droplet concentration with the advanced very high resolution radiometer, J. Appl. Meteorol. Clim., 33, 334–347, 1994. 13236

Quaas, J., Boucher, O., and Lohmann, U.: Constraining the total aerosol indirect effect in the LMDZ and ECHAM4 GCMs using MODIS satellite data, Atmos. Chem. Phys., 6, 947–955, doi:10.5194/acp-6-947-2006, 2006. 13234

Quaas, J., Ming, Y., Menon, S., Takemura, T., Wang, M., Penner, J. E., Gettelman, A., Lohmann, U., Bellouin, N., Boucher, O., Sayer, A. M., Thomas, G. E., McComiskey, A., Feingold, G., Hoose, C., Kristjánsson, J. E., Liu, X., Balkanski, Y., Donner, L. J., Ginoux, P. A., Stier, P., Grandey, B., Feichter, J., Sednev, I., Bauer, S. E., Koch, D., Grainger, R. G., Kirkevåg, A., Iversen, T., Seland, Ø., Easter, R., Ghan, S. J., Rasch, P. J., Morrison, H., Lamarque, J.-F., Iacono, M. J., Kinne, S., and Schulz, M.: Aerosol indirect effects – general circulation model intercomparison and evaluation with satellite data, Atmos. Chem. Phys., 9, 8697–8717, doi:10.5194/acp-9-8697-2009, 2009. 13234

Shao, H. and Liu, G.: A critical examination of the observed first aerosol indirect effect, J. Atmos. Sci., 66, 1018–1032, 2009. 13242

Skamarock, W. C., Klemp, J. B., Dudhia, J., Gill, D. O., Barker, D. M., Duda, M. G., Huang, X.-Y., Wang, W., and Powers, J. G.: A description of the advanced research WRF Version 3, National Center for Atmospheric Research, Boulder, Colorado, USA, 2008. 13260

Sorooshian, A., Feingold, G., Lebsock, M. D., Jiang, H., and Stephens, G. L.: On the precipitation susceptibility of clouds to aerosol perturbations, Geophys. Res. Lett., 36, L13803, doi:10.1029/2009GL038993, 2009. 13235

ACPD
14, 13233–13269, 2014

Stevens, B., Feingold, G., Cotton, W. R., and Walko, R. L.: Elements of the microphysical structure of numerically simulated nonprecipitating stratocumulus, J. Atmos. Sci., 53, 980–1006, 1996. 13239, 13260

Stevens, B., Lenschow, D. H., Vali, G., Gerber, H., Bandy, A., Blomquist, B., Brenguier, J., Bretherton, C. S., Burnet, F., Campos, T., Chai, S., Faloona, I., Friesen, D., Haimov, S., Laursen, K., Lilly, D. K., Loehrer, S. M., Malinowski, S. P., Morley, B., Petters, M. D., Rogers, D. C., Russel, L., Savic-Jovcic, V., Snider, J. R., Sraub, D., Szumowski, M. J., Takagi, H., Thornton, D. C., Tschudi, M., Twohy, C., Wetzel, M., and van Zanten, M. C.: Dynamics and Chemistry of Marine Stratocumulus–DYCOMS-II, B. Am. Meteorol. Soc., 84, 579–593, doi:10.1175/BAMS-84-5-579, 2003. 13238, 13260

Stevens, B., Moeng, C.-H., Ackerman, A. S., Bretherton, C. S., Chlond, A., De Roode, S., Edwards, J., Golaz, J., Jiang, H., Khairoutdinov, M., Kirkpatrick, M. P., Lewellen, D. C., Lock, A., Muller, F., Stevens, D. E., Whelan, E., and Zhu, P.: Evaluation of large-eddy simulations via observations of nocturnal marine stratocumulus, Mon. Weather Rev., 133, 1443–1462, 2005. 13260

Stevens, D. E., Ackerman, A. S., and Bretherton, C. S.: Effects of domain size and numerical resolution on the simulation of shallow cumulus convection, J. Atmos. Sci., 59, 3285–3301, 2002. 13260

Terai, C. R., Wood, R., Leon, D. C., and Zuidema, P.: Does precipitation susceptibility vary with increasing cloud thickness in marine stratocumulus?, Atmos. Chem. Phys., 12, 4567–4583, doi:10.5194/acp-12-4567-2012, 2012. 13235

Twohy, C. H., Petters, M. D., Snider, J. R., Stevens, B., Tahnk, W., Wetzel, M., Russel, L., and Burnet, F.: Evaluation of the aerosol indirect effect in marine stratocumulus clouds: droplet number, size, liquid water path, and radiative impact, J. Geophys. Res., 110, D08203, doi:10.1029/2004JD005116, 2005. 13242

Twomey, S.: The influence of pollution on the shortwave albedo of clouds, J. Atmos. Sci., 34, 1149–1152, 1977. 13235

Wang, H. and Feingold, G.: Modeling mesoscale cellular structures and drizzle in marine stratocumulus, Part I: Impact of drizzle on the formation and evolution of open cells, J. Atmos. Sci., 66, 3237–3256, 2009a. 13237, 13244, 13260

Wang, H. and Feingold, G.: Modeling mesoscale cellular structures and drizzle in marine stratocumulus, Part II: The microphysics and dynamics of the boundary region between open and closed cells, J. Atmos. Sci., 66, 3257–3275, 2009b. 13260

ACPD
14, 13233–13269, 2014

Wang, M., Ghan, S., Liu, X., L'Ecuyer, T. S., Zhang, K., Morrison, H., Ovchinnikov, M., Easter, R., Marchand, R., Chand, D., Qian, Y., and Penner, J. E.: Constraining cloud lifetime effects of aerosols using A-Train satellite measurements, Geophys. Res. Lett., 39, L15709, doi:10.1029/2012GL052204, 2012. 13235, 13236, 13239, 13243, 13244, 13245, 13247, 13251, 13252, 13261, 13264, 13267

Wang, S., Wang, Q., and Feinfold, G.: Turbulence, condensation, and liquid water transport in numerically simulated nonprecipitating stratocumulus clouds, J. Atmos. Sci., 60, 262–278, 2003. 13246, 13247

Xue, H. and Feingold, G.: Large-eddy simulations of trade wind cumulus: investigation of aerosol indirect effects, J. Atmos. Sci., 63, 1605–1622, 2006. 13246, 13250

Xue, H., Feingold, G., and Stevens, B.: Aerosol effects on clouds, precipitation, and the organization of shallow cumulus convection, J. Atmos. Sci., 65, 392–406, 2008. 13247

Yamaguchi, T. and Feingold, G.: Technical note: large-eddy simulation of cloudy boundary layer with the advanced research WRF model, J. Adv. Model. Earth Syst., 3, M09003, doi:10.1029/2012MS000164, 2012. 13238

ACPD
14, 13233–13269, 2014

Table 1. Data source description.

Campaign	Location	Reference	Cloud Type(s)	Model	Microphysics
ASTEX[a]	Northeastern Atlantic	Ackerman et al. (2004)	Nocturnal drizzling stratocumulus	Stevens et al. (2002), Ogura and Phillips (1962)	Ackerman et al. (1995)
DYCOMS-II[b]	Coastal Southern California	Ackerman et al. (2004)	Marine stratocumulus	Stevens et al. (2002), Ogura and Phillips (1962)	Ackerman et al. (1995)
FIRE-I[c]	Coastal Southern California	Ackerman et al. (2004)	Cloud field	Stevens et al. (2002), Ogura and Phillips (1962)	Ackerman et al. (1995)
RICO[d]	Antigua and Barbuda (Caribbean)	Lee et al. (2012)	Precipitating shallow cumulus	WRF[1] (Skamarock et al., 2008)	2-moment bulk (Feingold et al., 1998; Wang and Feingold, 2009a)
VOCALS-REx[e]	Southeast Pacific	Berner et al. (2011)	POCs	SAM[2] (Khairoutdinov and Randall, 2003)	2-moment bulk (Morrison and Gettelman, 2008)
DYCOMS-II[b]	Coastal Southern California	Wang and Feingold (2009a)	Marine stratocumulus	WRF[1] (Skamarock et al., 2008)	2-moment bulk (Feingold et al., 1998)
DYCOMS-II[b]	Coastal Southern California	Wang and Feingold (2009b)	Marine stratocumulus, ship tracks	WRF[1] (Skamarock et al., 2008)	2-moment bulk (Feingold et al., 1998)
RICO[d]	Antigua and Barbuda (Caribbean)	Jiang et al. (2010)	Precipitating shallow cumulus	RAMS[3] (Cotton et al., 2003)	bin (Feingold et al., 1996; Stevens et al., 1996)

[a] Atlantic Stratocumulus Transition Experiment
[b] second Dynamics and Chemistry of Marine Stratocumulus (Stevens et al., 2003, 2005)
[c] First ISCCP (International Satellite Cloud Climatology Project) Regional Experiment
[d] Rain in Cumulus over the Ocean
[e] VAMOS (Variability of the American Monsoon System) Ocean–Cloud–Atmosphere–Land Study - Regional Experiment
[1] Weather Research and Forecasting
[2] System for Atmospheric Modeling
[3] Regional Atmospheric Modeling System

ACPD
14, 13233–13269, 2014

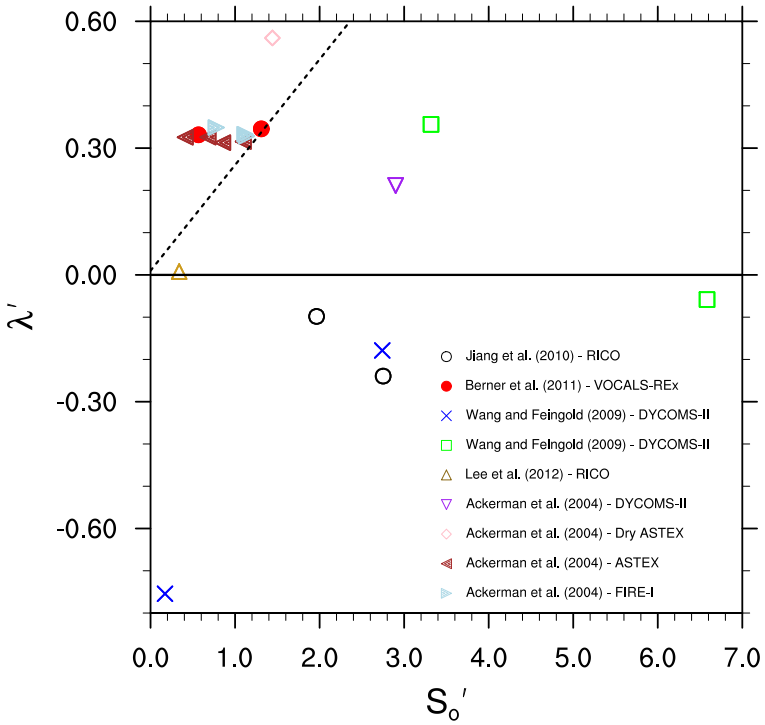

Figure 1. Scatterplot of λ' vs. S_o' from previously published studies. The legend provides the reference that corresponds to each symbol. Note here that "prime" notation is used because not all these studies provide enough detail to determine λ and S_o. Specifically, S_o' is $\mathrm{d}\ln R/\mathrm{d}\ln N_a$ in Jiang et al. (2010) and λ' is $\mathrm{d}\ln \mathrm{LWP}/\mathrm{d}\ln N_d$ in Berner et al. (2011). For all other references, $\lambda' = \lambda$ and $S_o' = S_o$. The thin dashed line shows the linear relationship determine by Wang et al. (2012) for the λ–S_{pop} relationship.

ACPD
14, 13233–13269, 2014

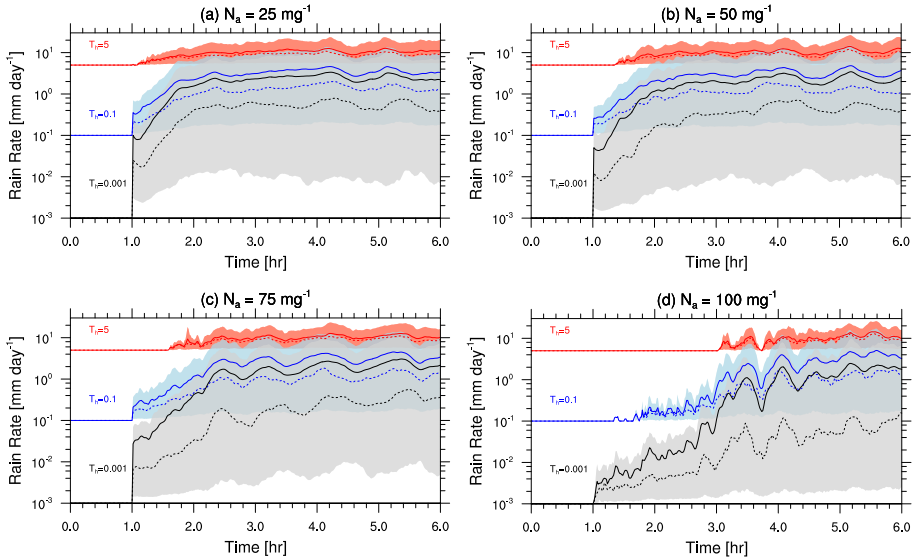

Figure 2. Mean (solid) and median (dashed) rain rates for the 3 rain rate thresholds, i.e., T_h of 0.001 (gray), 0.5 (blue), and 5 (red) mm day^{-1} for four different aerosol loadings. The shaded region encompasses the 10th percentile to the 90th percentile. R is depicted as equal to to T_h for the first hour as a reference point for the minimum R that is possible under each T_h condition.

ACPD
14, 13233–13269, 2014

Cloud and rain water responses to changes in aerosol

Z. J. Lebo and G. Feingold

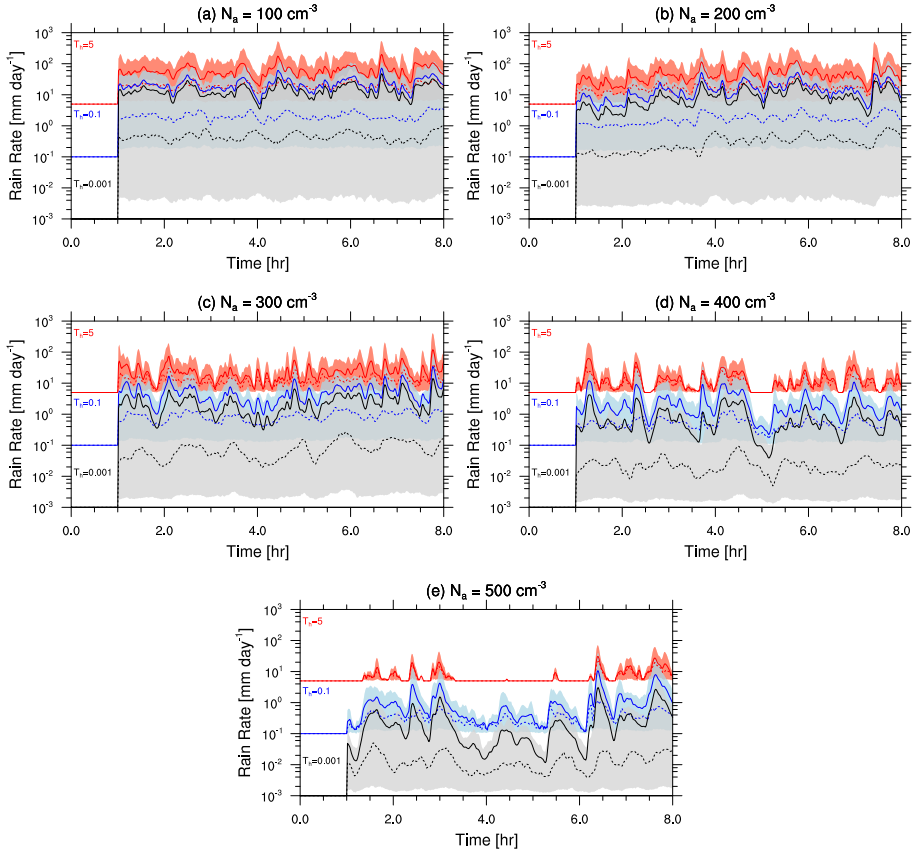

Figure 3. As in Fig. 2 except for the RICO case (the model output is from Jiang et al., 2010).

ACPD
14, 13233–13269, 2014

Cloud and rain water responses to changes in aerosol

Z. J. Lebo and G. Feingold

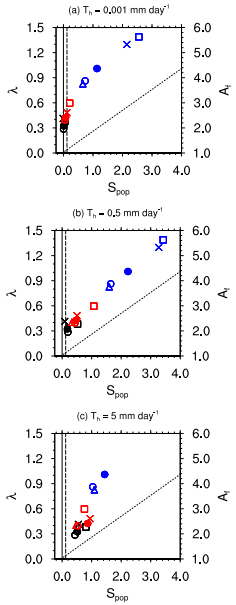

Figure 4. Scatterplot of λ (and A_f, right axis) vs. S_{pop} for thresholds T_h of **(a)** 0.001, **(b)** 0.5, and **(c)** 5 mm day^{-1}. These thresholds are representative of the set of 10 thresholds analyzed. Here, the following colors denote changes in N_a from 25 mg^{-1} to 50 mg^{-1} (black), 75 mg^{-1} (red), and 100 mg^{-1} (blue) for the DYCOMS-II case. The symbols signify the control (solid circles), Hi-LHF (open circles), Lo-LHF (crosses), Lo-CC (open squares), and Hi-CC (open triangles) simulations. Note that not all symbols appear, especially for larger changes in N_a and high threshold values because for those conditions no points met the criterion for calculating λ and/or S_{pop}. The thin dashed line shows the linear relationship determined by Wang et al. (2012) for the λ–S_{pop} relationship and the vertical dashed line corresponds to the satellite-measured value of S_{pop}, i.e., 0.12 (Wang et al., 2012).

ACPD
14, 13233–13269, 2014

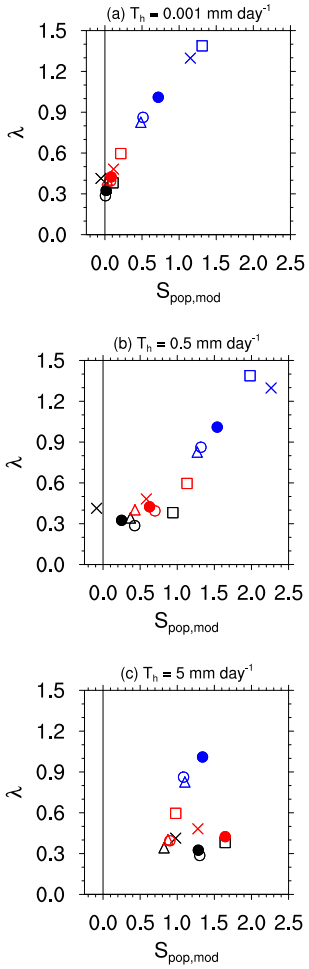

Figure 5. As in Fig. 4 except for λ vs. $S_{pop,\,mod}$, i.e., where the denominator in Eq. (3) is N_d.

ACPD
14, 13233–13269, 2014

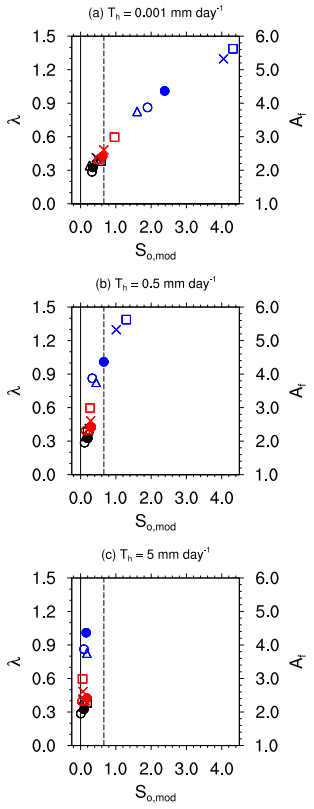

Figure 6. As in Fig. 4 except for λ vs. $S_{o,\,mod}$, i.e., where the denominators of the x- and y-axes are the same. The vertical dashed line corresponds to the surface remotely measured value of $S_{o,\,mod}$, i.e., 0.66 (Mann et al., 2014).

ACPD
14, 13233–13269, 2014

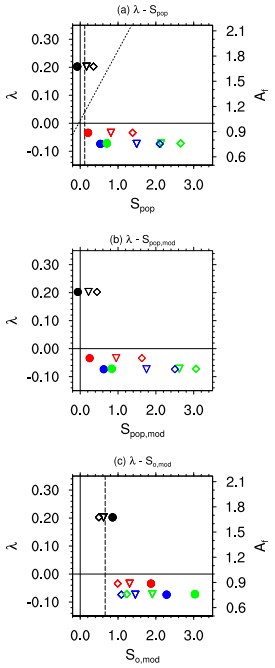

Figure 7. (a) λ (and A_f) vs. S_{pop}, **(b)** λ vs. $S_{pop,\,mod}$, and **(c)** λ vs. $S_{o,\,mod}$ for the RICO simulations from Jiang et al. (2010). The colors correspond to increasing N_a from 100 mg^{-1} to 200 (black), 300 (red), 400 (blue), and 500 (green) cm^{-3}. The symbols denote the different thresholds used to conditionally average R and POP, i.e., $T_h = 0.001$ (closed circle), 0.5 (downward pointing triangle, and 5 (diamond) mm day^{-1}. In **(a)**, the thin dashed line shows the linear relationship determined by Wang et al. (2012) for the λ–S_{pop} relationship and the vertical dashed line corresponds to **(a)** the satellite-measured value of S_{pop}, i.e., 0.12 (Wang et al., 2012) and **(c)** the surface-based estimate of $S_{o,\,mod}$, i.e., 0.66 (Mann et al., 2014).

ACPD
14, 13233–13269, 2014

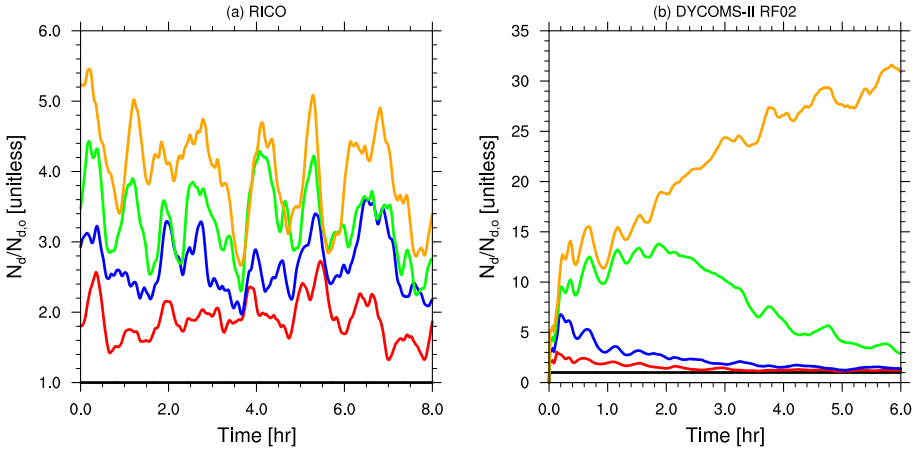

Figure 8. N_d relative to N_d for the lowest aerosol number concentration scenario (i.e., $N_{d,0}$) for both the **(a)** RICO and **(b)** DYCOMS-II RF02 simulations. Doubling (red), tripling (blue), quadrupling (green), and quintupling (orange) N_a are depicted for both sets of simulations. corresponding to $N_a = 200$, 300, 400, and 500 cm^{-3} relative to 100 cm^{-3}, respectively, for RICO and $N_a = 50$, 75, 100, and 125 mg^{-1} relative to 25 mg^{-1}, respectively, for DYCOMS-II RF02.

ACPD
14, 13233–13269, 2014

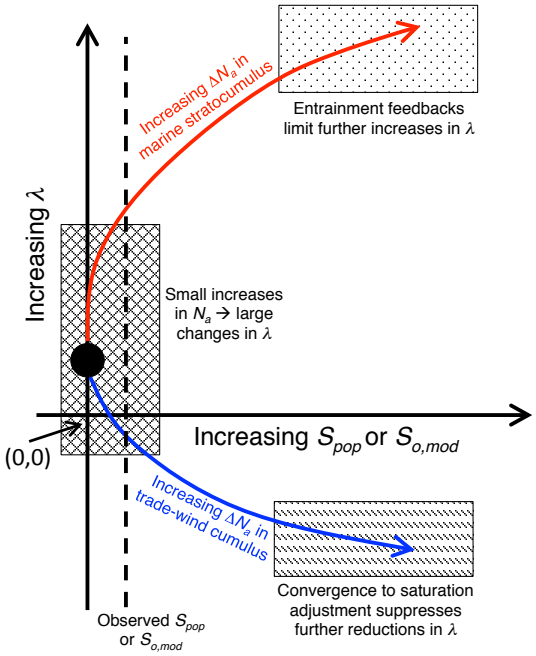

Figure 9. Schematic representation of the results presented herein. The red (blue) curve corresponds to the trajectory in the λ–S_{pop} parameter space for increasing changes in N_a (i.e., ΔN_a) in marine stratocumulus (trade-wind cumulus). The dotted region corresponds to the area of the parameter space where further increases in S_{pop} result in smaller changes in λ due to entrainment effects. The dashed region corresponds to the area in which the cloud microphysical characteristics asymptote to nearly constant values for larger ΔN_a. The crossed area represents the region in which λ changes rapidly relative to small changes in S_{pop}.

ACPD
14, 13233–13269, 2014